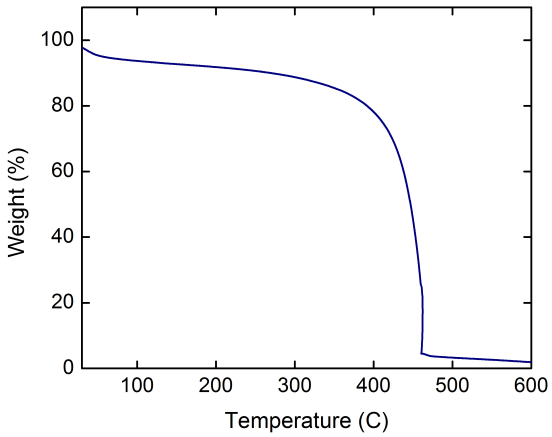

Figure 3.28 Thermo gravimetric analysis of the rGO hydrogel formed with the hydrothermal synthesis.

Chapter4. GRAPHENE BASED INKS FOR PRINTED ELECTRONIC APPLICATIONS

In this chapter novel graphene composites obtained for printed electronic applications are presented. A brief review on the materials for printed electronics like metal nanoparticles, polymers and polymers composites, is first introduced, then formulations of novel composites composed by an acrylic photocurable resin matrix with graphene as carbon filler will be presented and described together with electrical and morphological properties.
In the second part of the chapter the successful results of the use of graphene/acrylic resin composites as novel graphene based inks for Ink Jet printing applications are presented and several examples of prints on different substrates are showed. The results of morphological and electrical characterizations are reported and discussed. In the end preliminary results on piezoresistive properties characterization of graphene/polymer composites are also reported.

4.1 Background

Nowadays we are witnessing an increasing request for electronic devices production characterized by high demanding properties such as low manufacturing cost, long-time endurance, environmental sustainable production methods, recycling, low energy consumption, and high efficiency. Inkjet printing is one of the most promising low cost and environmentally sustainable manufacturing techniques for deposition of polymeric composites on flexible substrates (119). Several works report the application of inkjet printing technology to the fabrication of devices, which are more and more demanding in terms of manufacturing cost, environmentally friendly production methods, sustainable life cycle assessment of materials, which maintain state-of-the

art performance and characteristics. Several reviews dealing with new applications of inkjet printing technology are now available (120), (121).

Several materials have been tested for use as conductive inks (122), reporting different drawbacks. For instance, conductive polymers presented the disadvantage of relatively low conductivity (123), while metal nanoparticles (NPs) based inks need to be sintered at temperatures generally too high for application on most flexible substrates (124), (125). Temperatures as high as 300^oC may be potentially sustained by polyimide as high cost flexible substrate (126). Other examples of inkjet printable conductive materials are silver nanocomposite inks, which exploit UV curing to create the NPs in situ during the exposure, starting from a precursor (127), (128). In this case, there is no need to transfer heat to the system (129), (130), and cheap substrates (e.g., PP, PET, paper) may be used, even though the ultimate resistivity reached by those nanocomposites is suitable for resistor applications only (131) and not for conductive tracks, unless thermal sintering is performed. Polymeric materials seem to be the most promising candidates to meet all these challenges (132). In the inkjet printing, low viscosity should be maintained in the polymer precursor and fast polymerization needs to be performed soon after the deposition. For these reasons, the use of UV curing process seems to be very interesting because it is performed at room temperature, allowing the ink polymerization even on thermal sensitive substrates such as paper, and in addition is a fast overall manufacturing process (133). In order to decrease the surface resistivity of the dielectric polymer network, it is necessary to disperse conductive fillers in the precursor, to reach a conductive network (referring to the percolation theory, the so-called infinite cluster (134), which could ensure the requested electrical properties).

Printable inks based on conductive fillers are subjected to several constraints to meet specific conditions, to be ejected through nozzles of micrometric size (e.g. 20–80 μm). These include the optimization of rheological properties, ink viscosity, surface tension, and solvent evaporation rate (135)-(139). Carbon-based materials can be good candidates for conductive inks, due to their low cost and good electrical conductivity without the need of temperature treatments. This has been demonstrated for carbon nanotubes printed thin films (140), graphene bi- and tri-layer used as protective coating against oxidation on copper NPs-based inks (141), and in

graphene/water suspensions (142). Because of its high specific surface area, good chemical stability, electrical and thermal conductivity, and high charge carrier mobility (20 m^2 V^{-1} s^{-1}) (143), (144), graphene is actually the most suitable candidate to be dispersed in photo-curable formulations to obtain a UV-cured conductive ink. So far, the manufacturing of graphene-based polymer composites required not only that graphene sheets were produced on a sufficient scale, but also that they were incorporated, and homogeneously distributed, into various polymeric matrices as single layers. However, graphite, although inexpensive and available in large quantity, unfortunately does not readily exfoliate to yield individual graphene sheets, as already discussed in Chapter 2. A widely investigated alternative is the use of graphite oxide, a layered material produced by the oxidation of graphite (145), (146).

Simple and easily synthesized inks can be fabricated using graphene oxide (GO), which is strongly hydrophilic and can be easily dispersed in water-based solutions (147). In fact, in contrast to graphene, GO surfaces are heavily oxygenated presenting hydroxyl and epoxide functional groups on their basal planes, in addition to carbonyl and carboxyl groups at the sheet edges (148), (149). The advantage of the described formulations lies in the use of graphene oxide, which is easily dispersible in water-based solutions and can be reduced by UV irradiation (151). This allowed the fabrication of test samples by directly inkjet printing a polymeric formulation containing graphene oxide, which was subsequently cross-linked during the UV irradiation step.

4.2 Experimental Session: Synthesis of Graphene Oxide/Polymer Composites

In the next sections the possibility of introducing aqueous dispersion of GO into acrylic resin matrices, such as poly(ethylene glycol) diacrylate (PEGDA), thus fabricating a conductive printable ink which is environmentally friendly, will be explored. The reduction of GO is performed using UV light irradiation, which allowed the simultaneous photopolymerization of the polymeric matrix (151), that acts as a binder. Structural and electrical characterizations

showed the efficiency of the reduction method and promising values of conductivity of printed test patterns. The possibility of introducing GO fillers into acrylic resin matrices (poly(ethylene glycol) diacrylate, PEGDA) will be shown, and the structural and electrical characterization of the UV-cured printed composite that will show the efficiency of the reduction method and promising values of conductivity.

In next sections is also reported the electrical characterization of an inkjet-printed composite material based on PEGDA matrix filled with GO, achieved in real-time during the irradiation with UV light. The mechanism for resistance drop achieved during UV irradiation due to the reduction of the GO filler will be discussed. These results open the way to the application of graphene-based polymeric composite inks, relatively easy to synthesize, directly printable at room temperature on flexible substrates and readily usable without further sintering.

4.2.1 Graphene Oxide/PEGDA UV-Curable Formulations

4.2.1.1 Material and Methods

Only commercial reagents were used: graphene oxide (thickness 0.71.2 nm) was purchased from Cheap Tubes Inc. (USA) and used without further purification, PEGDA (poly ethylene glycol diacrylate) with Mw = 575 g mol^{-2} was purchased from Sigma-Aldrich and Darocur 1173 radical photoinitiator (PI) from BASF. The formulations were prepared by adding 0.5 g of PEGDA and 0.08 g of PI to 4.5 g of DI water in which 0.02 g of GO was previously dispersed (corresponding to the GO/PI ratio of 1/4).

The procedure for the preparation of thick films of about 100 μm thickness of a GO/PEGDA/PI composites is reported in Figure 4.1, where is shown that after combining all the three components and mixing them in order to obtain an homogeneous slurry, the mixture was deposited on a microscope slide glass using a wire-wound bar and subsequently exposed to UV light for 5 min. As a reference for electrical characterization, a PEGDA/PI thick film was similarly prepared without adding the GO.

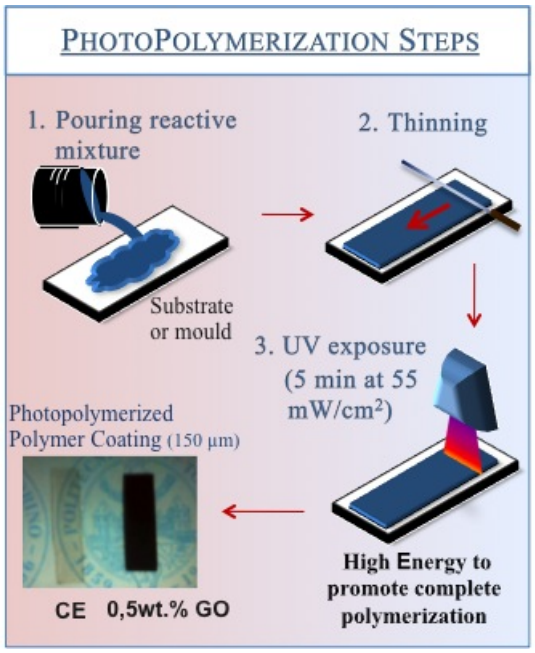

Figure 4.1 Photo-polymerization steps process.

4.2.1.2 Results and Discussion

The poly ethylene glycol diacrylate is an UV-curable acrylic resin with formula showed in Figure 4.2. It was chosen as polymeric matrix due to its non-toxicity and water solubility properties, to synthetize an environmentally friendly formulation with graphene oxide. The photoinitiator that is needed to create reactive species that help starting the photopolymerization process of the PEGDA is the Darocur 1173, already presented in chapter 3.

Thick films starting from the GO/PEGDA/PI formulations were prepared following the pro-

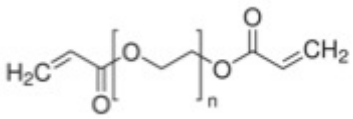

Figure 4.2 poly ethylene glycol diacrylate with Mw = 575 g mol^{-2}

cedure described in the Material and Methods section. Electrical characterizations were performed on the films, and in Figure 4.3 are reported the electrical values calculated with a four-probe measurement of surface resistance. It is possible to notice that the value of the surface resistance decrease with the increase of the graphene content, confirming the effective-

Sample	Rs[a] ($\Omega.sq^{-1}$)
PEGDA	$> 10^{11}$
PEGDA + 0.5 wt.-% GO	$> 10^{11}$
PEGDA + 1 wt.-% GO	5×10^{6}
PEGDA + 2 wt.-% GO	6 300

Figure 4.3 Four-probe measurements of surface resistance

ness of the increase of the conductivity values of the polymer matrix by having a carbon filler in it.

The reduction of GO to graphene driven by UV irradiation was demonstrated by X-ray photoelectron spectroscopy as previously reported in chapter 3 in Figure 3.11. The occurrence of a single-step procedure starting from a homogeneous aqueous dispersion of GO, which undergoes reduction induced by the UV radiation during photopolymerization of the acrylic resin allowed to observe a significant decrease in intensity of the peaks associated with carbonyl groups normally present on GO surfaces, evidencing the photoinduced GO reduction with restoration of the extended conjugated sp^2 structure (150).

The advantage of the described formulations lies in the use of graphene oxide, which is easily dispersible in water-based solutions and can be reduced by UV irradiation (151). In Figure 4.1 it is shown the comparison between the graphene compound and the pure polymeric matrix to put in evidence the much darker color of the compound material respect to the pure polymeric matrix, due to the carbon filler. In order to understand the micro morphology of the samples, FE-SEM characterization has been performed and in Figure 4.4 and Figure 4.5 are reported respectively the top surface and the cross section of the film made of the compound rGO/PEGDA after the UV-irradiation. On the top part of the film it is possible to notice some of the graphene flakes embedded in the polymeric matrix and in the cross-section picture, in Figure 4.5, is clearer how the graphene sheets are positioned all across the thickness of the film, that in this is about 45 μm. This graphene/polymer composite can be also used

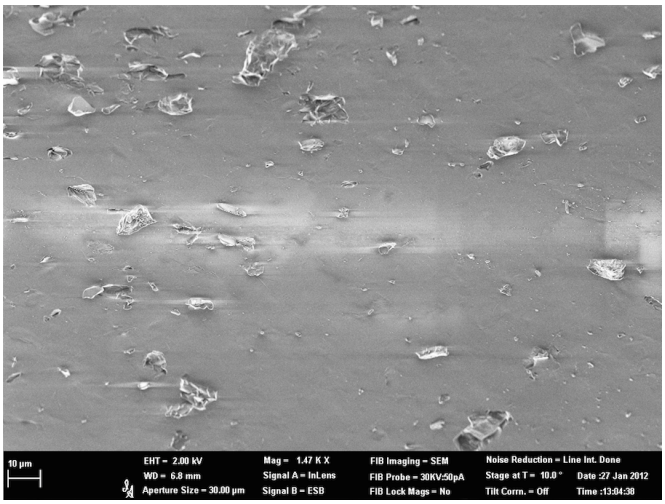

Figure 4.4 SEM image showing the top surface microstructure of the thick rGO/PEGDA film after the UV-irradiation.

for the preparation of aqueous acrylic formulations of variable viscosity, which are suitable for the fabrication of inkjettable UV-curable inks.

4.2.2 Graphene Oxide/PEGDA Inks for Ink Jet Printing Applications

4.2.2.1 Material and Methods

The formulation of the graphene based ink followed the same procedure described in the previous Material and Methods section. 0.5 g of PEGDA and 0.08 g of PI to 4.5 g of DI water in which 0.02 g of GO was previously dispersed (corresponding to the GO/PI ratio of 1/4). These formulations were tested in a MicroFab Inkjet Printer with automatic 3D position control, showed in Figure 4.6, using an 80 μm piezoelectric nozzle vibrating at a frequency of 250 Hz, at room temperature.

The typical electrical pulse applied to the piezoelectric actuator is a trapezoidal waveform (positive only or positive followed by a negative). The transitions from one voltage level to the other reduce/increase the cross-section of the tube capillary and produce pressure variations (with respect to resting conditions) of the fluid enclosed in the tube. Jetting parameters were set using an asymmetrical pulse, and in Figure 4.7 is reported a graph of the tension signal

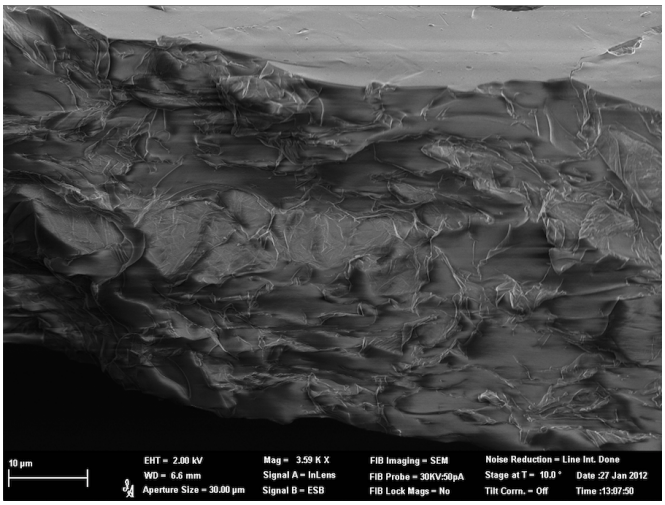

Figure 4.5 SEM image showing the cross-section microstructure of the thick rGO/PEGDA film after the UV-irradiation.

Figure 4.6 Ink Jet printer used for the experiments, with parameters fluid viscosity: 1-20 cP, drop volume: 10 pl 1 nl, nozzle diameter: 20-100 μm, drop velocity: 3 10 ms^{-1}.

applied to the piezoelectric component. The paramenters used consist in idle voltage 3 V, dwell voltage 35 V, and echo voltage 35 V and, the signal parameters used were: first rise time 6 ms to let start the initial fluid expansion, dwell time 40 ms for pressure wave propagation, fall time 25 ms for fluid compression, echo time 40 ms and second rise time 3 ms used to cancel the residual acoustic waves propagating. The bipolar asymmetrical pulse is normally preferred to facilitate droplet formation and ejection, see Figure 4.8. The second part of the waveform can be used to cancel some of the residual acoustic oscillations that remain in the device after drop ejection.

Straight line patterns were printed on glass slides and several values of resolution and thick-

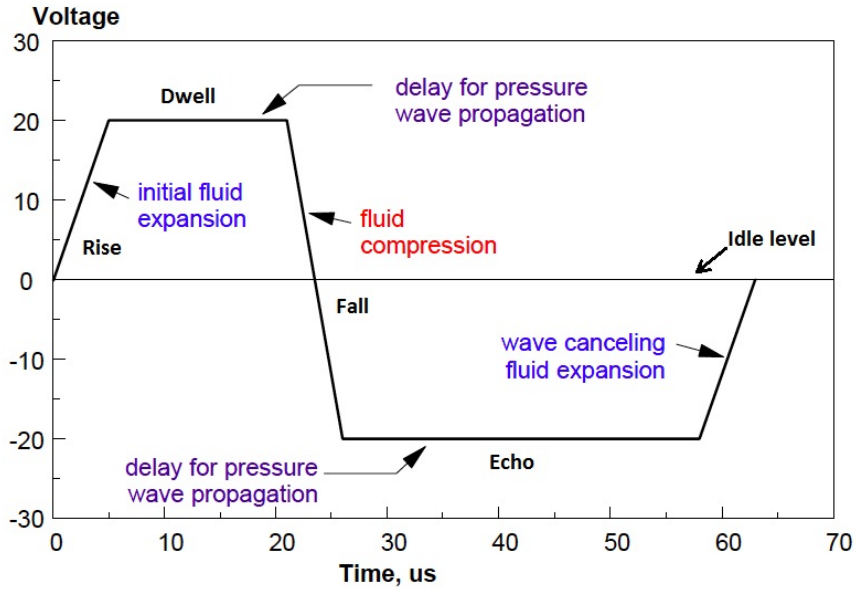

Figure 4.7 Ink Jet printer tesion signal applied to the piezoelectric coponent for the control of the drop ejection.

ness were tested. The dimension and speed of ink drops were controlled using a horizontal camera located onto the xy stage for direct drop observation. Using the described printing setup, ink drops with a diameter of 100 μm were normally obtained. Since resolution is not an issue, in this study devoted to the characterization of the UV-induced reduction, we did not optimize the ejection parameters, which normally enable a printing resolution beyond 50 μm. A drop spacing of 200 μm was used to achieve complete coverage of the patterned substrate.

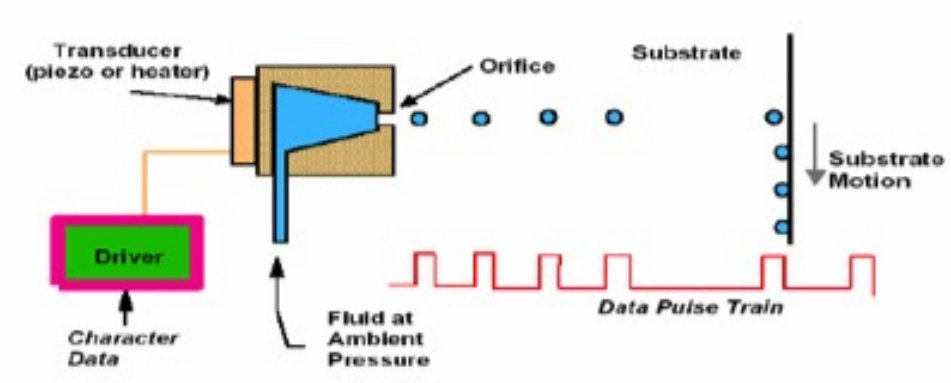

Figure 4.8 Ink Jet printer mechanism process.

subsequently exposed to UV light for 2 min.

Current/voltage (IV) measurements were performed on thick and printed films using a standard two-point micro-contact setup of a Keithley 2635 A multimeter. The structural analysis and morphology of thick and thin printed films were characterized by optical and scanning electron microscopy (SEM). The electrical characterization was performed on all samples at room temperature, in the range -200 to +200 V. Resistivity was computed comparing GO/PEGDA thick films with printed thin films of several thicknesses (varied with dpi resolution and repetition of printing on the same track, measured by profilometry). These measurements were planned to assess the variation in resistivity due to GO reduction to graphene by UV irradiation, and any potential collateral effects produced by the high strain rate to which inks are submitted to in the printing nozzle.

4.2.2.2 Results and Discussion

In the experiments conducted, conductive printable inks, based on aqueous acrylic UV-curable formulations containing GO were investigated. The oxide can be easily dispersed in water and it can be reduced during UV irradiation, with the simultaneous build up of the crosslinking network. The polymer network acts as a binder during printing and the in situ reduced GO decreases the resistivity of the acrylic polymer, forming a conductive percolative network. This GO/PEGDA/water ink was tested by inkjet spotting straight line patterns with variable resolution (85-190 dots-per-inch, dpi) and repetition of passes on the same track (from 1 to 5) on paper, as shown in Figure 4.9. Several test patterns of the GO/PEGDA formulations were inkjet printed also on transparent substrates (microscope glass slides) as shown in Figure 4.10, where it is shown an optical microscope magnification of a printed track with 125 dpi and 3 passes that generated tracks 10μm thick and 500μm wide.

The thickness of printed films was varied either by increasing the spotting resolution (variation of dpi) or repeating the same track in multiple passes, up to five times. In particular, the repeated tracks showed a good uniformity and coverage of the substrate. The structure of printed tracks was characterized by observation using an optical microscopy while the thick-

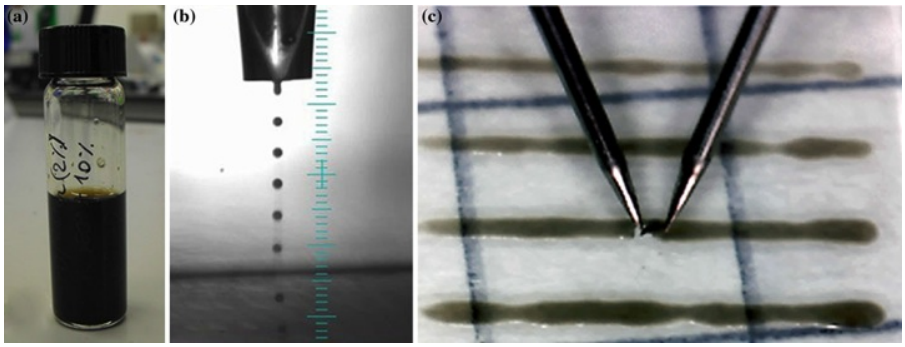

Figure 4.9 GO/PEGDA/water ink (a), InkJet nozzle printing GO/PEGDA/water ink (b), and the two-point micro-contact setup for IV measurements used for inkjet printed GO thin films (c)

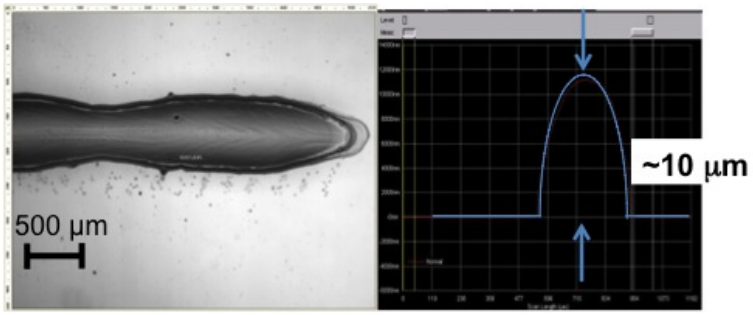

Figure 4.10 Structural inspection of RGO/PEGDA inkjet-printed tracks on a glass slide after UV irradiation: top-view optical microscopy image of a 500 μm wide track (a) and a profilometry scan showing a thickness of about 10 μm (b)

ness uniformity was inspected by profilometry, as shown in Figure 4.10. The top view and line profile of a typical PEGDA/GO track printed on a glass slide substrate (after polymerization) showed good uniformity and coverage of the substrate and the thickness wa measured using a profilometer.

The analysis of the microstructure of the printed tracks demonstrates that GO flakes distribute uniformly on the substrate and form a continuous layer with each other, ensuring continuity of electrical signal (Figure 5.4).

The electrical response of printed thin films (PEGDA/GO) was compared with one of the thick films (PEGDA/GO and PEGDA reference) fabricated by wire-wound bar. Figure 4.12 shows the raw (not normalized to layer resolution/thickness) IV characteristics of those samples. Figure 4.9 shows a typical setup of the measurement for inkjet printed thin film.

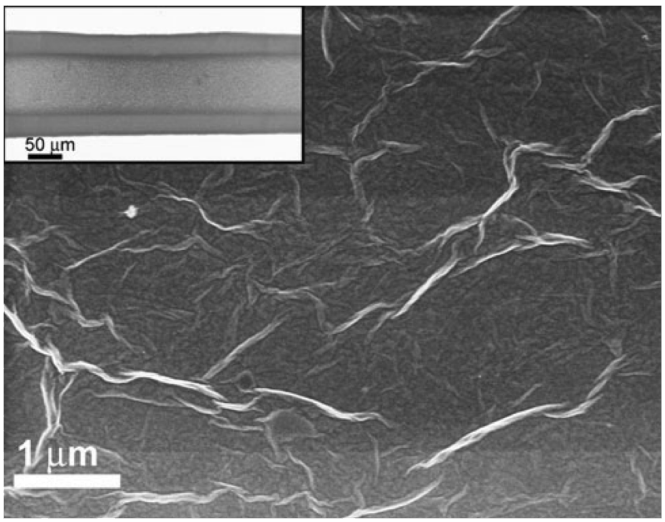

Figure 4.11 SEM image showing the microstructure of an inkjet printed track of PEGDA/GO track. The inset shows a low-resolution image of the printed track

The IV response of the thin inkjet printed track features an absolute current which accidentally appears in the same range of the pure matrix thick film. This effect obviously depends on the difference in size and thickness of thick and thin printed films. Remarkably, the PEGDA/GO thick film shows a non-linear response, strongly different from the other materials: since the electrical response (at least in the DC regime) may be interpreted in terms of superposition of different contributions, the nonlinear effect can be expected to come from either the PEGDA matrix or the reduced GO filler. Nonetheless, neither the pure PEGDA matrix nor the inkjet printed sample show such a nonlinear trend, allowing to conclude that in the thick wire-wound bar-fabricated sample there should still exist a fraction of unreduced GO, possibly due to the complete absorption of UV radiation in a few micrometers at the top of the sample.

This phenomenon, leading to inhomogeneous samples in the direction perpendicular to the film plane, was already observed on different classes of materials featuring UV in situ reduction processes (143), (146). These phenomena are thought to be due to the shielding effect originating by the filler (in our case, the GO flakes) which limits the light penetration depth, and therefore hinders the UV-induced GO reduction. Figure 4.13 shows the resistivity of thin printed layer samples as a function of sample thickness, compared to thick films of PEGDA/GO and pure PEDGA. Each experimental point in the plot is given by a computation based on linear fits to

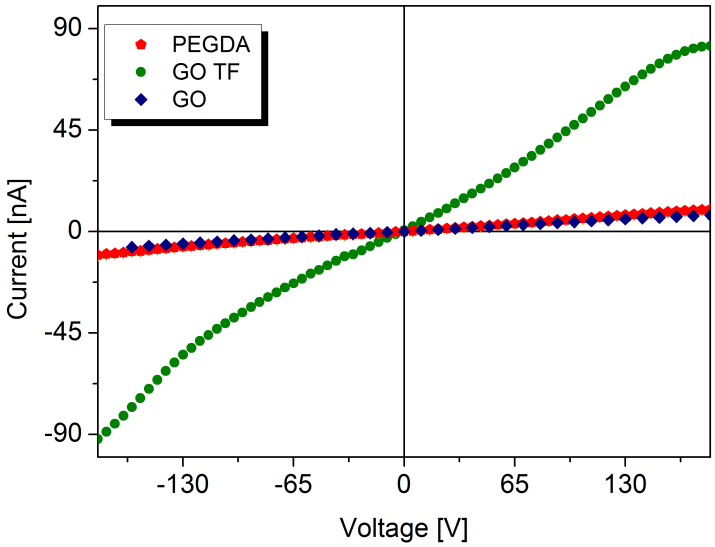

Figure 4.12 Raw IV characteristics of pure PEGDA and GO thick films (TF), and GO inkjet printed thin film.

average IV curves (error bars shown in the plot). The addition of GO to PEGDA, after reduction by UV irradiation, results in a decrease of resistivity by over an order of magnitude (GO TF versus PEGDA TF). For what concerns printed samples, two trends may be evidenced, both concurring to a resistivity decrease. By increasing the number of passes and thus the track thickness, a small decrease of resistivity is obtained (green dashed arrow in Figure 4.13); this fact is normally due to an increased volume available for electrons drift. Furthermore, by decreasing the amount of ink spotted on a single-pass track (i.e., reducing the dpi resolution) and thus reducing the line thickness, a strong reduction of GO is obtained (blue solid arrow in Figure 4.13). Those samples show a decrease of resistivity by two orders of magnitude with respect to the pure matrix. This counter-intuitive fact may be explained considering that in a thin track a higher fraction of GO is reached and reduced by UV light than in a thick track, thus better contributing to electrical conduction (143), (146).

The analysis of coefficients of dispersion as a function of the film thickness (Figure 4.14), computed by fitting IV curves with a linear function, demonstrates that all samples ideally follow the Ohms law (within 0.4 %). Only the GO thick film sample appears out of scale, if compared

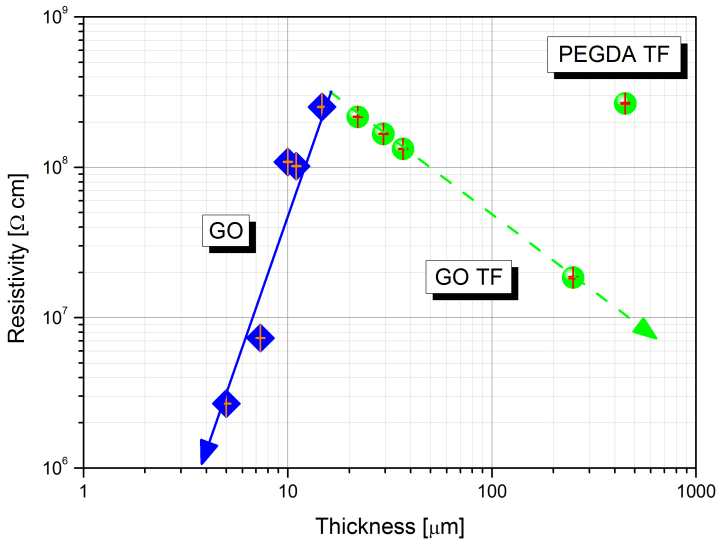

Figure 4.13 Resistivity of GO inkjet printed and thick film (TF) samples, as computed from linear fit to IV curves, as a function of the sample thickness. Error bars are shown on experimental data points. The series refer to the inkjet printed tracks with single (blue solid arrow) and multiple (green dashed arrow) passes

to thin inkjet printed samples and to pure PEGDA matrix (Ohms law likelihood around 1.5 %). This confirms the nonlinear behavior of thick films and the shielding effect previously described for Figure 4.12.

In-situ I-V characherizations Real-time current/voltage measurements were performed in order to assess the variation in resistivity due to photo-polymerization of the PEGDA matrix and concurrent GO reduction to graphene driven by UV irradiation. A standard two-point setup was built, connecting two sides of a metalized kapton sheet having a 1 mm gap between the electrodes; a Keithley 2635A multimeter was used to establish a fixed voltage (5 V) across the electrodes. The electrical characterization was performed on all samples at room temperature, during the UV-irradiation phase, inside the static UV lamp, making use of an electrical feedthrough. The samples were irradiated using several values of UV light power densities (50, 70 and 85 mW/cm^2). Data were not converted in resistivity, but kept in current, due to the difficulty in determining the real sample thickness, particularly when in liquid (not poly-

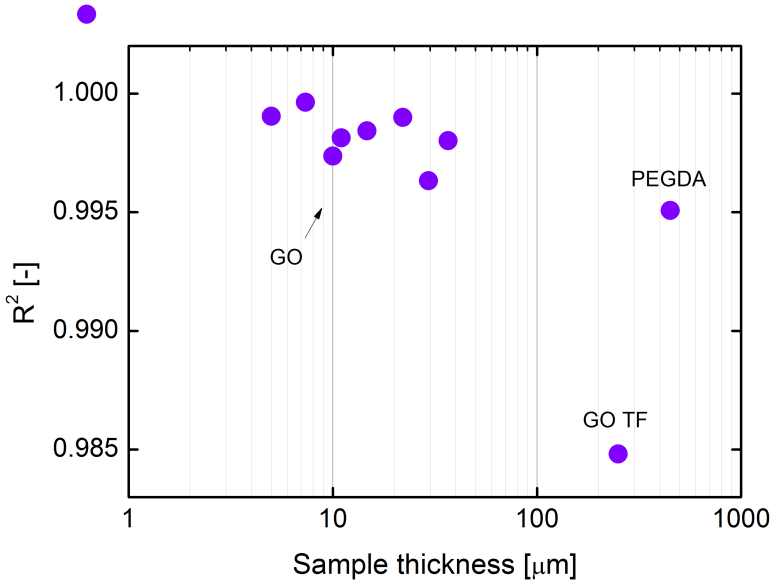

Figure 4.14 Analysis of the coefficients of dispersion as a function of the film thickness: GO are the ink jet printed tracks, GO TF are the thick fim of the GO/PEGDA compound and the PEGDA the pure matrix.

merized) phase. The precursor/precursor suspension including GO was inkjet printed in the electrode gap before starting current acquisition. The structural integrity of printed films was characterized by optical microscopy after UV exposure.

The electrical measurements performed in situ during the step of polymer cross-linking/GO reduction allowed to monitor the mechanism of reaction which led to the reduction of the overall resistivity of the printed composite toward the values measured for the pure polymer matrix. UV irradiation tests were repeated using three different UV light power densities, confirming the behavior described in the previous section. Figure 4.15 reports the variation of resistance of printed samples of PEGDA/GO composite, as a function of the UV irradiation time, starting from time = 0 corresponding to the as-printed non-polymerized matrix. The values are expressed as a function of the starting value of resistance R_0 measured for the nonpolymerized matrix.

It can be easily inferred that there is a trend in resistance drop, depending on the energy supplied to the system. In fact, the lowest value of resistance is achieved with the highest value of UV light power density. Figure 4.16 reports the variation of sample resistance with time,